

The Formation of Protective Nitride Surfaces for PEM Fuel Cell Metallic Bipolar Plates

M.P. Brady, B. Yang, H. Wang, J.A. Turner, K.L. More, M. Wilson, and F. Garzon

The selective gas nitridation of model nickel-based alloys was used to form dense, electrically conductive and corrosion-resistant nitride surface layers, including TiN, VN, CrN, Cr₂N, as well as a complex NiNbVN phase. Evaluation for use as a protective surface for metallic bipolar plates in proton exchange membrane fuel cells (PEMFC) indicated that CrN/Cr₂N based surfaces hold promise to meet U.S. Department of Energy (DOE) performance goals for automotive applications. The thermally grown CrN/Cr₂N surface formed on model Ni-Cr based alloys exhibited good stability and low electrical resistance in single-cell fuel

cell testing under simulated drive-cycle conditions. Recent results indicate that similar protective chromium nitride surfaces can be formed on less expensive Fe-Cr based alloys potentially capable of meeting DOE cost goals.

INTRODUCTION

Proton exchange membrane fuel cells (PEMFCs) are of interest for power generation due to their high efficiency and near-zero emissions.¹⁻⁵ They are typically based on an ion-conductive sulphonated fluoropolymer membrane such as Nafion® and operate in the 60–80°C temperature range.¹ Applica-

tions range from portable power (cell phones, laptops, etc.) to automobiles and on-site power-generation systems. Cost and durability concerns are the key barriers to their widespread use.¹⁻⁵

PEM FUEL CELLS AND BIPOLAR PLATES

Among the most expensive components in PEMFCs, and the dominant weight and volume of the fuel cell stack, are the bipolar plates (Figure 1).¹⁻⁵ The bipolar plates serve to electrically connect the anode of one cell to the cathode of another in a stack to achieve a useful voltage. They also separate and distrib-

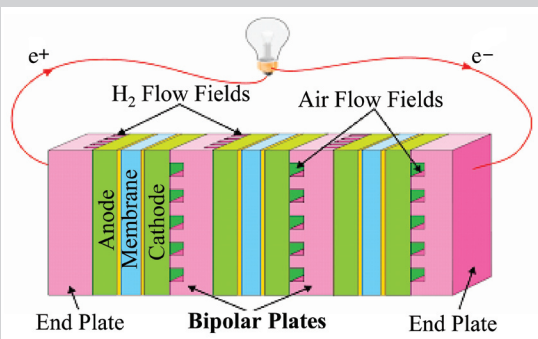


Figure 1. A schematic of a three-cell fuel cell stack showing bipolar plates (artwork from Reference 6, courtesy of Los Alamos National Laboratory and the U.S. Department of Energy). Each fuel cell delivers on the order of only 0.6–0.9 V under typical operating conditions.¹ In practice, tens to hundreds of fuel cells can be stacked together to achieve useful voltage levels.

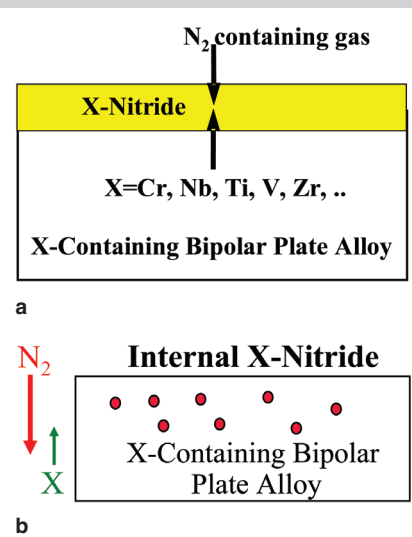


Figure 2. A schematic of limiting cases for thermal nitridation based on the classic Wagner Oxidation Theory. (a) Continuous, external layer formation, (b) internal precipitate formation.

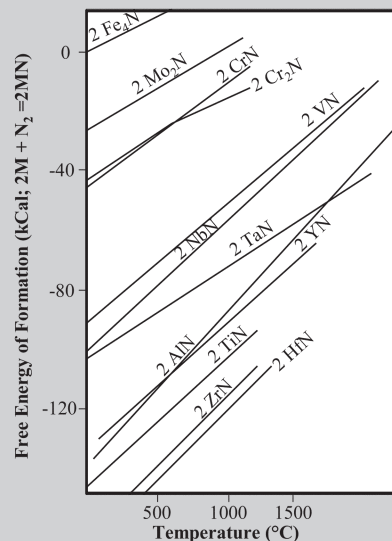


Figure 3. A schematic Ellingham-Richardson diagram for nitride stability (based on and redrawn from diagrams reported in References 47 and 48). Nitrides of nickel are typically not stable on reaction with N₂ at atmospheric pressures, and would lie above Fe₂N on this diagram. Note that AlN was not pursued as a protective layer for metallic bipolar plates due to its poor electrical conductivity.

ute reactant and product streams. To accomplish this, flow-field grooves are manufactured into the faces of the plates (Figure 1). Graphite is the benchmark material for bipolar plates because it is electrically conductive and corrosion resistant in the highly aggressive anode and cathode PEMFC environments (60–80°C acidic conditions, containing F⁻ leached from the membrane). However, the brittleness and relatively high gas permeability of graphite necessitates the use of thick plates (>2–5 mm), which lowers the power density of the fuel cell stack.^{1–5} Machining of flow fields into graphite plates is also expensive, making graphite impractical for most wide-scale commercial uses. Developmental bipolar plate materials under investigation include graphite/carbon-based composites,^{7–10} polymer-based composites with conductive graphite/carbon fillers,^{11–16} and metals.^{17–38}

The U.S. Department of Energy (DOE) has set technical targets for bipolar plates for automotive applications (Table I).³⁹ Thus far, no material has definitively established itself as capable of meeting all the target properties for the desired lifetimes of >5,000 h under drive-cycle conditions. The graphite/carbon and polymer-based composites generally exhibit excellent corrosion resistance in PEMFC environments. However, the graphite/carbon composites^{3–5,7–10} typically have to be sealed to reduce gas permeability, have brittleness issues, and can be difficult to produce at thicknesses <1 mm to achieve the high power densities desired for automotive applications. The manufacture of graphite/carbon composites can also be costly, especially when measures are taken to mitigate their property shortcomings. To meet automotive cost goals, bipolar plates need to be less than ~\$1–\$2 for a ~500 cm² plate. The polymer-based composites are the current state of the art for bipolar plates and are available commercially.^{3–5,11–16} Cost targets appear achievable, but thus far through-thickness conductivities are inadequate for automotive applications. Currently available plates typically exhibit conductivities of only ~20–30 S/cm, whereas the DOE goal is >100 S/cm. Better conductivities appear to be achievable with very high loadings of conductive phase additions (graphite or carbon particles, fibers, nanotubes, etc.),

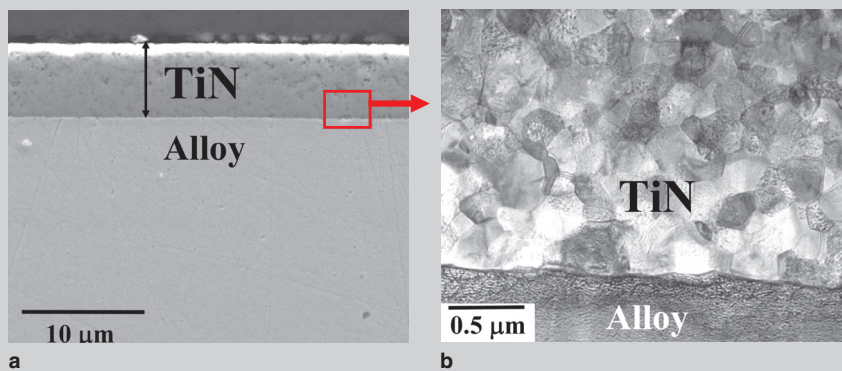


Figure 4. Cross sections of Ni-10Ti (wt.%) after 48 h at 1,100°C in N₂.^{43,50} (a) Scanning-electron microscopy (SEM) image; (b) scanning-transmission-electron microscopy (STEM) image of nitride layer.

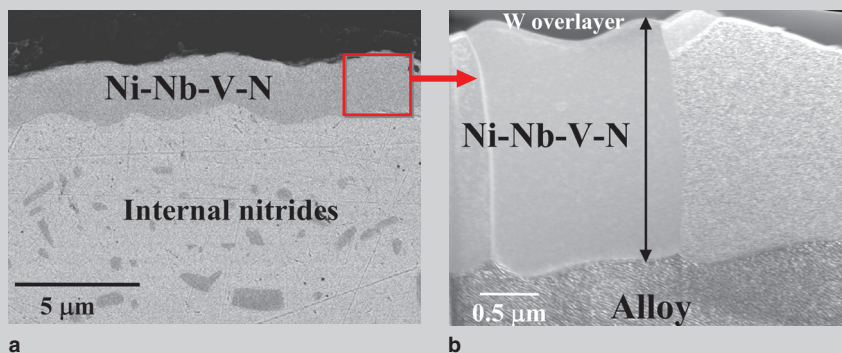


Figure 5. Cross sections of Ni-10Nb-5V (wt.%) after 24 h at 1,100°C in N₂. (a) An SEM image; (b) STEM image of nitride layer.⁵⁰

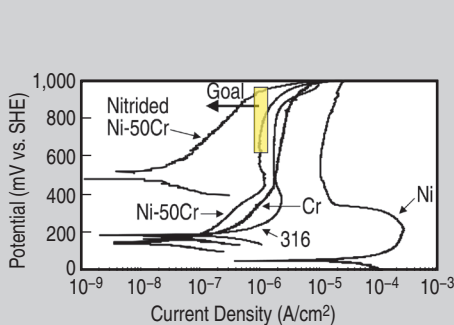


Figure 6. Polarization data in aerated pH 3 sulfuric acid at 80°C (scan rate of 0.1 mV/s) vs. SHE.^{43,55,56}

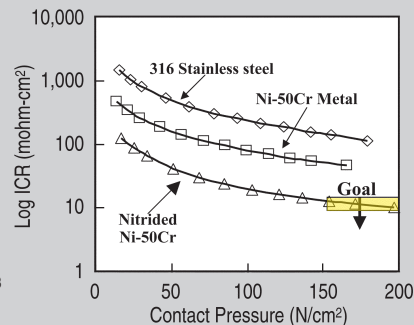


Figure 7. Interfacial contact resistance data.^{55,56}

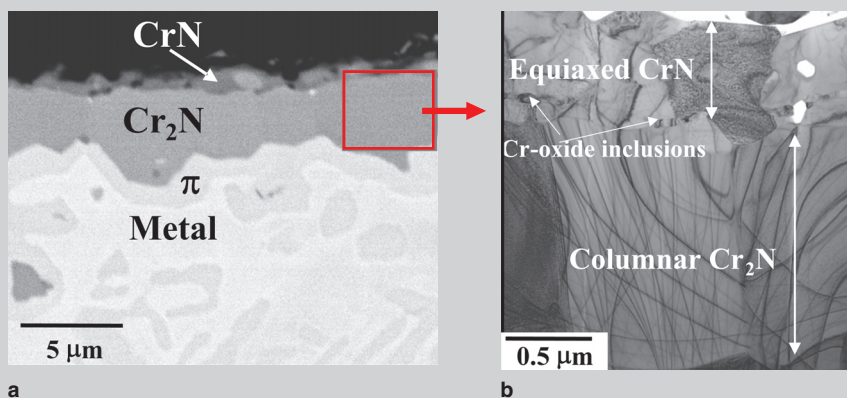


Figure 8. Cross sections of nitrided Ni-50Cr (wt.%) (1,100°C, 2 h, N₂) after 4,100 h exposure in a bipolar corrosion test cell.^{54–56} (a) An SEM image of the cathode-exposed face⁵⁶ and (b) TEM image of the nitride.⁵⁵ The fine black lines on the columnar Cr₂N in the TEM image are bend contours caused by electron scattering through the buckled sample.

Table I. DOE Technical Targets: Bipolar Plates³⁹

Characteristic	Units	Status	
		2004	2010
Cost	\$/kW	10	6
Weight	kg/kW	0.36	<1
H ₂ Permeation Flux	cm ³ sec ⁻¹ cm ⁻² @ 80°C, 3 atm (equivalent to <0.1 mA/cm ²)	<2 × 10 ⁻⁶	<2 × 10 ⁻⁶
Corrosion	μA/cm ²	<1 ^a	<1 ^b
Electrical Conductivity	S/cm	>600	>100
Area-Specific Resistance ^c	Ohm cm ²	<0.02	0.01
Flexural Strength	MPa	>34	>4 (crush)
Flexibility	% deflection at mid-span	1.5 to 3.5	3 to 5

a–Based on coated metal plates; b–may have to be as low as 1 nA/cm² if all corrosion product ions remain in ionomer;
c–includes contact resistance.

although this can make the plates more difficult to manufacture. The high loadings also tend to make the plates brittle, especially when making thin plates on the order of 0.5 mm to 1 mm thick. Despite their current limitations, graphite/carbon and polymer-based composite bipolar plates remain promising candidates, and a number of public and private sector development efforts are currently under way to address their shortcomings.

See the sidebar on page 54 for details on metallic bipolar plates.

THERMALLY GROWN NITRIDE COATINGS

A possible solution to forming a defect-free protective surface on metallic bipolar plates is to grow a protective nitride layer from the bipolar plate alloy by high-temperature nitridation.⁴³ Transition metal nitrides⁴⁴ offer an attractive combination of high electrical conductivity and good corrosion resistance, which makes them of interest for protective coatings for metallic bipolar plates.² In thermal nitridation, the goal is to design the alloy and set the reaction conditions such that the desired nitride-forming element diffuses outward from the alloy to react with the nitriding gas to form a continuous surface layer (Figure 2a). Pin-hole defects are not an issue because, at elevated temperatures, thermodynamic and kinetic factors favor the reaction of all metal surfaces exposed to the nitriding gas.⁴³ As such, it is also not line-of-sight limited and is amenable to use with complex-shaped surfaces such as the edges and corners of the flow field grooves in bipolar plates (Figures 1 and A).

The drawback of the thermal nitridation approach is that it is very substrate-alloy dependent and it can be difficult to control the composition and morphology

of the nitride that is formed. For example, if the alloy composition or nitridation conditions are not selected properly, discrete internal nitride precipitates (Figure 2b), which would not provide corrosion protection, can form instead of the desired external, continuous nitride surface layer (Figure 2a). Further, even if a continuous nitride surface layer can be formed, cracking of the layer can occur on cooling due to the thermal expansion mismatch between the nitride and the substrate alloy. Control of such phenomena is the basis for protective oxide scale formation by heat-resistant alloys (e.g., References 45 and 46), but has not previously been well explored as a synthesis method to form protective nitride surface layers. The proposed thermal nitridation approach is different from the more familiar conventional ferrous alloy nitridation to achieve surface hardening, whereby conditions are set to diffuse nitrogen extensively into the alloy to form iron nitrides and/or nitrogen-saturated iron-based phases tens to hundreds of micrometers deep. The goal of bipolar plate protection is to form an external, continuous nitride layer no more than a few micrometers thick.

Exploratory work was performed with the nitridation of model Ni-X alloys, where X = Cr, Nb, Ti, V, and Zr to form CrN, Cr₂N, NbN, TiN, VN, ZrN, etc., phases.⁴³ Nickel was chosen as the initial alloy base because it does not form a stable nitride under typical nitridation conditions (Figure 3) and has a low permeability to nitrogen, which, based on classic Wagner Oxidation Theory (reviewed in References 45, 46, and 49), favors the formation of a continuous, external nitride layer on nitridation rather than discrete internal nitride precipitates (Figure 2). At the

time this work was initiated (2000), the cost of nickel was also relatively low (~\$2–3/lb), and potentially able to meet DOE automotive cost goals. In recent years, the price of nickel has significantly increased (~\$6–10/lb), leaving nickel-based alloys too expensive for PEMFC bipolar plate automotive applications. However, the primary purpose of these studies was proof-of-principle evaluation of the thermal nitridation approach, and to identify which nitride compounds had the most promise for protection in PEMFC environments.

Nitride formation was explored in the temperature range of 800–1,200°C in N₂ and N₂-4H₂ environments, rather than conventional surface-hardening nitriding conditions of ~500–600°C in NH₃, which produces a highly effective nitrogen activity and favors internal penetration of nitrogen. Some representative nitrided microstructures are shown in Figures 4 and 5.^{43,50} A continuous, external ~10 μm thick layer of TiN was readily formed on Ni-10Ti (wt.%) (Ni-12Ti [at.%]) after exposure at 1,100°C for 48 h in N₂ (Figure 4a). The microstructure consisted of a highly planar nitride/alloy interface, with submicrometer, equiaxed grains of TiN of composition Ti-(45–50)N (at.%) (Figure 4b). Such a microstructure is indicative of conditions favoring nitride nucleation over growth, and is consistent with the expected high driving force for nucleation due to the high thermodynamic stability of Ti/TiN relative to nickel (Figure 3). Detailed studies of nitride formation in Ni-Ti alloys by Savva et al.⁵¹ indicate that the transition from internal to external TiN in Ni-Ti alloys occurs at titanium levels as low as ~Ni-(1–2)Ti (wt.%) (1–2.5 at.% Ti) at 1,020°C.

At the opposite end of the spectrum, a coarse-grained, columnar microstructure (Figure 5) was formed on Ni-10Nb-5V (wt.%) (Ni-6.5Nb-6V [at.%]) after exposure under similar conditions (1,100°C, 24 h, N₂) to Ni-10Ti (wt.%).⁵⁰ Both continuous external nitride layer formation and internal nitride formation were evident. Efforts to form an NbN layer on binary Ni-Nb alloys were not successful, with very little reaction with nitrogen observed. Additions of vanadium were made in an attempt to increase reactivity with nitrogen, as Ni-V alloys readily formed VN surface layers. Vanadium

was also selected because VN is of intermediate thermodynamic stability between nickel and NbN (Figure 3), via the so-called third-element effect, whereby ternary additions of intermediate stability can help promote the formation of a protective surface layer at alloy concentrations lower than in the corresponding binary alloys. (The classic example of this phenomenon is chromium additions to Ni-Al and Fe-Al alloys, which lower the level of aluminum needed to form a protective Al_2O_3 scale on thermal oxidation relative to binary Ni-Al and Fe-Al alloys; the third element effect is reviewed in References 45 and 46). Interestingly, rather than an NbN surface layer, a complex nitride of composition Ni-(12–15)V-(15–20)Nb-(20–30)N (at.%) was formed on nitrated Ni-10Nb-5V (wt.%).⁵⁰ X-ray diffraction analysis indicated that both the alloy and the complex nitride were face-centered cubic structures (Fm3-m), suggesting that the Ni-Nb-V-N composition and columnar structure may be more the result of a solid-solution type reaction path than an exclusive selective nitridation process.

The corrosion resistance of the nitride surface layers was assessed by polarization in pH 3 sulfuric acid solutions at 80°C to simulate PEMFC operating conditions.⁴³ Corrosion current densities of less than 1×10^{-6} A/cm² up to ~0.9 V vs. standard hydrogen electrode (SHE) under aerated conditions (to simulate the cathode-side environment) and -0.2 to +0.1 V vs. SHE under H_2 -purged conditions (to simulate the anode-side environment) were considered sufficiently promising to warrant further investigation. Relatively low corrosion current densities were observed for the TiN surfaces formed on Ni-Ti based alloys, but post-test analysis revealed local areas of through-thickness attack in some coupons.⁴³ This seemed to correlate with TiN thickness, and was less prevalent with thinner TiN layers (<1–2 μm). The VN and Ni-Nb-V-N surfaces were less corrosion resistant under these conditions, with corrosion current densities in the 10^{-5} to 10^{-4} A/cm² range at <0.9 V vs. SHE under aerated conditions.⁴³ Among the nitrated surfaces/nitrides evaluated, only CrN/Cr₂N consistently exhibited the target corrosion current densities.⁴³

PROTECTIVE Cr-NITRIDE SURFACES ON MODEL Ni-Cr-BASED ALLOYS

Nitridation studies of binary Ni-Cr alloys have indicated little reactivity with nitrogen at low levels of chromium; however, as the chromium level is increased, nitrogen permeability (which favors internal rather than external nitride formation) also increases,⁵² such that levels of chromium in excess of ~30–35 wt.%^{53,54} are needed to form an external, continuous nitride. Therefore, Ni-50Cr was used as a model material to evaluate the behavior of thermally grown chromium-nitride surfaces. Polarization data for nitrated Ni-50Cr (1,100°C, 2 h, N_2) in aerated pH 3 sulfuric acid at 80°C is shown in Figure 6, and interfacial contact resistance (ICR) data in Figure 7.^{43,55,56} The corrosion resistance of nitrated Ni-50Cr was significantly better than that of Ni-50Cr metal and pure chromium, pure nickel, and type 316 stainless steel (~18Cr-10Ni [wt.%] base) shown for comparative purposes. Nitridation also lowered the ICR of Ni-50Cr ~fivefold, to the DOE target value of 10 mohm-cm² at contact pressures of 150–200 N/cm², which is an order of magnitude lower than that of 316 stainless steel.

Figure 8 shows the microstructure of nitrated Ni-50Cr after a 4,100 h exposure in a bipolar corrosion test cell using pH 3 sulfuric acid with 2 ppm F⁻ at 80°C, with one coupon face exposed to a solution purged with air and the other with H_2 .⁵⁵ The nitrated structure consisted of a thin, equiaxed CrN layer overlying a dense, columnar Cr₂N layer. Significant internal nitridation also occurred. No attack of the nitride surface was evident, despite the long-term corrosion exposure. There was also no increase in ICR compared with the as-nitrated surface.

Based on these promising corrosion and ICR screening results, single-cell fuel cell testing was pursued for nitrated Ni-50Cr. A simple serpentine 50 cm² active area plate architecture was adopted, using thick Ni-50Cr anode and cathode plates designed to duplicate graphite test plate hardware (Figure 9a). Full nitride surface coverage was readily achieved across all edge, corner, and flow field features, with no evidence of CrN/Cr₂N layer cracking or loss of adherence. These plates were initially run for 500 h

under constant 0.7V conditions (80°C). There was no plate resistance increase or loss of performance. Analysis of the membrane electrode assembly (MEA) by x-ray fluorescence (XRF) indicated no metallic ion contamination within the detection limits of the measurement, of the order of $\sim 0.1\text{--}1 \times 10^{-6}$ g/cm². This result provides evidence that thermal nitridation can protect irregular surface features such as corners, edges, holes, and flow field grooves.

The nitrated Ni-50Cr plates were then subjected to an additional ~1,160 h of drive-cycle testing using a cycle of 0.94 V for 1 min., 0.60 V for 30 min., 0.70 V for 20 min., and 0.50 V for 20 min. An additional 24 full shutdowns (cell cooled off, gases removed, and opened to air at connections) were superimposed in an attempt to induce even more aggressive conditions. No loss of performance was observed; in fact, performance slightly increased during drive cycle testing (Figure 9b). A small amount of nickel contamination of the MEA, 2×10^{-6} g/cm², was, however, detected. This small amount of nickel was likely the result of leaching from occasional, local regions of the CrNiN π phase^{57–59} that were initially formed during nitridation, instead of the more protective CrN/Cr₂N surface.⁵⁴ No attack of the CrN/Cr₂N surface was evident. (Such local π phase formation can occur at regions of significant chromium depletion in cast Ni-50Cr.) Overall, proof-of-principle exploratory corrosion, ICR, and single-cell fuel cell studies indicated that thermally grown CrN/Cr₂N surfaces show good potential to meet DOE bipolar plate performance and durability goals.

EXTENSION OF PROTECTIVE Cr-NITRIDE FORMATION TO Fe-Cr-BASED ALLOYS

With the current high cost of nickel (~\$6–10/lb), Ni-Cr based alloys cannot meet DOE automotive cost goals. Therefore, efforts were initiated to form similar protective CrN/Cr₂N surfaces on Fe-Cr based alloys by thermal nitridation. This is difficult because at commercially viable levels of chromium, less than ~30 wt.% chromium due to the σ phase field, the permeability of nitrogen in Fe-Cr alloys is sufficiently high that internal chromium-nitride precipitates are gen-

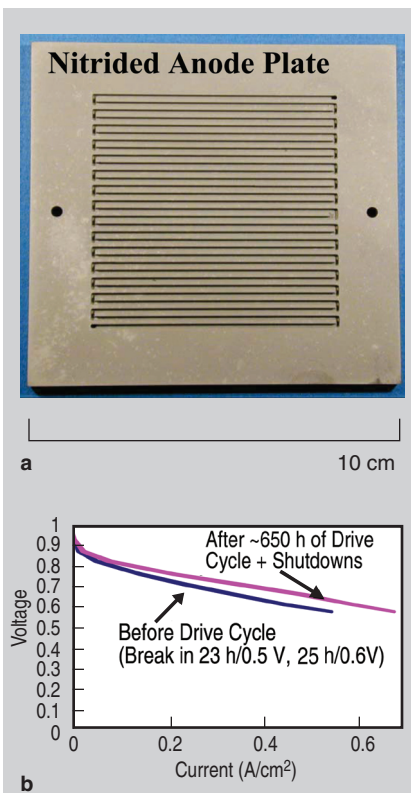


Figure 9. Single-cell fuel cell testing of nitrated Ni-50Cr (1,100°C, 2 h, N₂-4H₂) anode and cathode plates. (a) Typical nitrated plate; (b) performance curves.

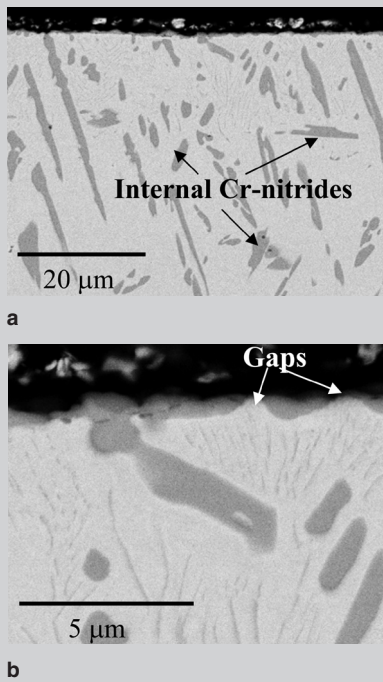


Figure 10. Scanning-electron microscopy cross sections of Fe-27Cr (wt.%) exposed for 4 h at 900°C in flowing, purified N₂-4H₂. (a) Low-magnification view showing internal chromium-nitride formation (dark phase); (b) high-magnification view of alloy surface region showing discontinuous chromium-nitride surface (dark phase).

erally favored rather than the desired external, continuous chromium-nitride layer (Figures 2b and 10).^{60,61} Nitridation in model Fe-27Cr (wt.%) based alloys as a function of ternary alloying additions and nitridation environment (N₂ partial pressure, H₂ level, O₂-impurity level, and temperature) was studied in an attempt to form a dense, external chromium-nitride surface. A ferritic based alloy was chosen rather than an austenitic based alloy to eliminate the need for costly nickel additions, with 27 wt.% chromium chosen because it is representative of the type 446 family of high-chromium, commercial stainless-steel alloys.

Under some conditions, oxygen impurities present in an N₂-4H₂ nitriding environment resulted in the formation of a thin (submicrometer) Cr₂O₃ layer on heat-up to the nitriding temperature (850–900°C). This occurred because Cr₂O₃ is much more stable thermodynamically than the chromium nitrides, with only 5–10 ppm of O₂ impurities in N₂-4H₂ needed to form oxide. The

initially formed Cr₂O₃ layer was found to be highly effective in limiting internal nitridation of binary Fe-27Cr, with subsequent conversion of the external chromium oxide surface to external chromium nitride as the oxygen impurities in the nitriding environment were consumed.⁶¹ The resulting microstructure was a semi-continuous chromium-nitride overlying the remaining chromium oxide, but exhibited borderline to unacceptably high corrosion rates.

However, the use of initial oxide formation to limit internal nitridation proved highly effective in Fe-27Cr alloys modified with 2 wt.% and 6 wt.% vanadium.⁶¹ In the Fe-27Cr-2V and 6V alloys, O₂ impurities in the nitriding environment resulted in the initial formation of a (V,Cr)₂O₃ surface layer during heat-up, which was subsequently converted to a dense, fully continuous vanadium-doped chromium-nitride surface layer, overlying an intermixed oxide/nitride region. Corrosion resistance and ICR values comparable to the nitrated Ni-50Cr

METALLIC BIPOLAR PLATES

Metallic alloys such as stainless steels would be ideal as bipolar plates (e.g. References 26–30) because they are amenable to low-cost/high-volume manufacturing methods such as stamping, offer high thermal and electrical conductivities, have low gas permeability and excellent mechanical properties, and can be readily made in foil form (~≤ 0.1 mm thick) to achieve high power densities (Figure A). The primary limitations are high contact resistance and borderline corrosion resistance and cost. Despite bulk electrical conductivities which are orders of magnitude greater than the U.S. Department of Energy (DOE) goal of >100 S/cm, stainless steels generally exhibit interfacial contact resistance (ICR) values an order of magnitude higher (worse) than the DOE goal of 10 mohm-cm² (e.g., References 28–30). This is due to the passive oxide layer present on stainless steels, which is the source of their corrosion resistance. On exposure to the highly aggressive proton exchange membrane fuel cell (PEMFC) environments, especially on the aerated cathode side, further growth of the oxide layer and even higher ICR values can result.^{28–30} Dissolution of metallic ions from stainless steels can also occur under PEMFC operating conditions, especially in the reducing anode side environment where protective oxide film formation can be difficult, and under cyclic operating conditions at high voltages such as those encountered in automotive applications (e.g., References 2–5, 25, 31, and 32). Sulphonated fluoropolymer membranes are very sensitive to poisoning by metallic ions, and cell performance can be significantly degraded.^{2–5,25,31,32}

The degradation in fuel cell performance from metallic ion dissolution and contamination depends on the complex interaction of a number of factors, including the degree of capture of the metallic species in the membrane, its specific interaction with the membrane, the chemistry of the membrane, and the fuel cell stack cell design and operating conditions.^{2–5,25,31,32} A rough estimate would be that contamination levels of the order of only 10–100 ppm of metallic ions are a significant concern for performance degradation. For some PEMFC applications and operating conditions/durability requirements, untreated stainless steel alloys may provide acceptable performance and durability. However, for automotive applications, the high ICR and borderline corrosion resistance are not acceptable, at least with conventional fuel cell designs. The rising costs of stainless-steel alloy components, especially nickel, also leaves many compositions unable to meet cost goals. Other metallic materials have also been investigated as bipolar plate materials, particularly Ni-Cr, titanium, and refractory metals such as niobium and tantalum (e.g., References 2, 22, 37, and 43). However, the cost of these materials is generally in excess of DOE automotive goals, and ICR values and/or corrosion resistance are still borderline with respect to the DOE targets. They remain candidates for some

were achieved. Vanadium was effective because VN has greater stability relative to V_2O_3 than does CrN relative to Cr_2O_3 (approximately 100 ppm O_2 is required to form oxide on vanadium in N_2-4H_2 at $900^\circ C$ vs. ~ 10 ppm for chromium), which aided conversion of the initially formed oxide to nitride. Vanadium is also readily soluble in Fe-Cr alloys, and V_2O_3 - Cr_2O_3 , CrN-VN, and Cr_2N - V_2N are all, respectively, mutually soluble. (Formation of V_2O_5 , which is toxic and exhibits a low melting point, was not observed under the conditions studied.)

The promising results obtained with nitrated Fe-27Cr-2V and Fe-27Cr-6V (wt.%) were accomplished in a sealed nitriding environment, dependent on a narrow range of O_2 impurity levels, and proved difficult to reproduce consistently.⁶¹ Preoxidation studies are currently under investigation to solve the reproducibility issues by controllably introducing a defined level of oxide formation prior to nitridation, and to further investigate the proposed reaction

mechanism. Figure 11 shows polarization data in aerated pH 3 sulfuric acid at $80^\circ C$ for Fe-27Cr-6V (wt.%) nitrated after preoxidation in flowing Ar- $2O_2$ or Ar- $10N_2+O_2$ impurities, followed by nitridation in flowing O_2 -gettered N_2-4H_2 . Corrosion current densities were in the range of the nitrated Ni-50Cr. The ICR values for preoxidized/nitrated Fe-27Cr-6V met the DOE goal of 10 mohm-cm² at a contact pressure of only ~ 100 N/cm² (Figure 12), which is somewhat better (lower) than those for nitrated Ni-50Cr (Figure 7). Corrosion screenings were also conducted under aggressive conditions of aerated pH 0 $H_2SO_4 + 2$ ppm F^- at $70^\circ C$ held for 7.5 h at 0.84 V vs. SHE. Interfacial contact resistance values increased slightly (Figure 12), but still met the DOE goal at contact pressures of only ~ 100 N/cm². A scanning-electron microscopy (SEM) cross section of the nitrated Fe-27Cr-6V alloy preoxidized in Ar- $10N_2+O_2$ impurities is shown in Figure 13. It consisted of external vanadium-doped chromium

nitride with finger-like projections into an inner region of V-Cr oxide, consistent with $(V,Cr)_2O_3$ (identification based solely on SEM and energy-dispersive x-ray analysis in this sample). Little internal nitridation was evident.

The use of oxide to aid in external nitride formation is a concern with regards to through-thickness electrical conductivity. The ICR data reported in this paper were determined by measuring the voltage drop from a coupon placed between copper plates and carbon contact paper as a function of compaction pressure^{28-30,55,56,60} and showed no indications of limited through-thickness conductivity. The intermixed nature of

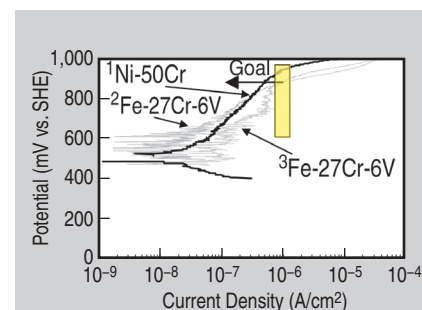


Figure 11. Polarization data in aerated pH 3 sulfuric acid at $80^\circ C$ (scan rate of 0.1 mV/s) vs. SHE for preoxidized and nitrated Fe-27Cr-6V vs. Ni-50Cr. ¹Ni-50Cr: $1,100^\circ C$, 2 h, N_2 ; ²Fe-27Cr-6V: preoxidized at $900^\circ C$ for 8 h in flowing Ar- $10N_2 + O_2$ impurities followed by $900^\circ C$ for 24 h in flowing, purified N_2-4H_2 ; ³Fe-27Cr-6V: preoxidized at $800^\circ C$ for 20 min. in flowing Ar- $2O_2$ followed by $900^\circ C$ for 24 h in flowing, purified N_2-4H_2 .

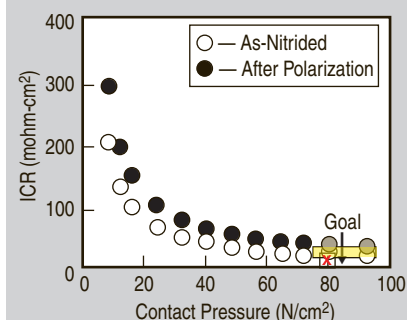


Figure 12. The ICR data for Fe-27Cr-6V preoxidized at $900^\circ C$ for 8 h in flowing Ar- $10N_2 + O_2$ impurities followed by $900^\circ C$ for 24 h in flowing, purified N_2-4H_2 . As-nitrated and after a 7.5 h hold in aerated pH 0 sulfuric acid + 2 ppm F^- at 0.84 V vs. SHE. Note that the plotted ICR values include resistance contributions from both major coupon faces. The data are typically divided by 2 to obtain ICR; in this case that was not possible as only one major coupon face was exposed to the sulfuric acid.

portable or stationary applications, where cost targets and/or operating conditions may be less severe.

To meet DOE bipolar plate targets for automotive applications, metallic bipolar plates will require conductive and corrosion-resistant coatings or surface treatments. Unfortunately, coatings for metallic bipolar plates have thus far not proven sufficiently viable due to local areas of inadequate surface coverage (i.e., pin-hole defects),⁴⁰ which result in local corrosion and metallic ion contamination of the membrane. For many non-fuel-cell applications, such coating defects are not a significant issue. However, due to the sensitivity of the sulphonated fluoropolymer membranes to poisoning by metallic ions and the aggressiveness of the PEMFC operating environment, bipolar plates require a fully dense, essentially defect-free protective coating. This is especially true for low-cost but less corrosion-resistant metal substrates such as low-alloy steels or aluminum, which can be rapidly attacked in PEMFC environments.^{2-5,24,41} Methods to mitigate the presence of pin-hole defects (i.e., the use of interlayers) are being pursued (e.g., Reference 33), but can significantly increase costs. Difficulties are also encountered in obtaining full coverage of complex flow field corner and edge geometries. Emerging approaches include the use of claddings on low-cost substrates⁴² and the use of low-ICR coatings or surface treatments that are used in combination with stainless-steel alloy substrates to provide corrosion resistance.^{20,21,23,60}



a



b

Figure A. Metallic bipolar plate flow field features can be manufactured by high-volume manufacturing methods such as stamping. (a) Stamping of metallic bipolar plates; (b) stamped flow-field features. (Photographs courtesy of GenCell Corporation, Southbury, Connecticut.)

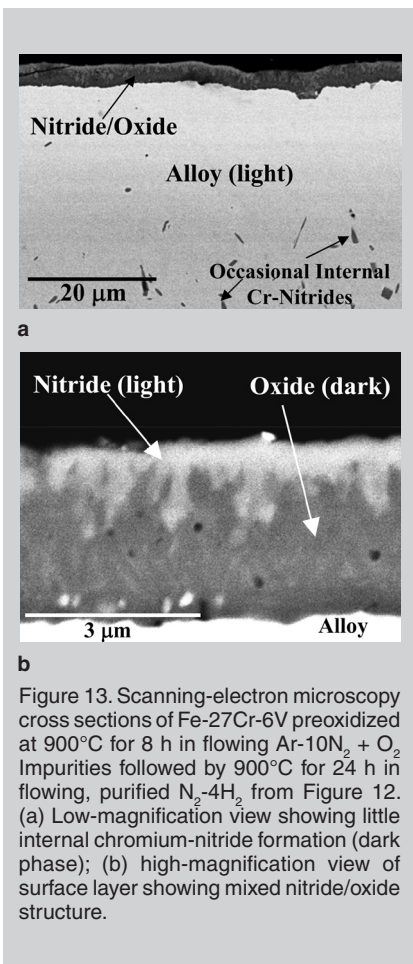


Figure 13. Scanning-electron microscopy cross sections of Fe-27Cr-6V preoxidized at 900°C for 8 h in flowing Ar-10N₂ + O₂ impurities followed by 900°C for 24 h in flowing, purified N₂-4H₂ from Figure 12. (a) Low-magnification view showing little internal chromium-nitride formation (dark phase); (b) high-magnification view of surface layer showing mixed nitride/oxide structure.

the nitride/oxide and N-doping and/or partial conversion of the oxide still present to nitride or oxy-nitride likely resulted in high-conductivity through-thickness paths. V₂O₅ is also highly conductive for an oxide.⁶² Above room temperature and/or on doping with chromium, there is a transition to more insulating behavior. However, resistivity values are still of the order of only ~2 ohm-cm at chromium levels of 10 at.% substitution for vanadium in (V,Cr)₂O₃,⁶² although chromium levels in some regions of the (V,Cr)₂O₃ formed on the Fe-27Cr-6V exceeded 10 at.%. It should be noted that preoxidized and nitrified binary Fe-27Cr coupons also showed low ICR values despite inner Cr₂O₃-based layers on the order of 0.5 μm thick⁶¹ (Cr₂O₃ is not conductive at room temperature). This result indicates that either there were also high-conductivity paths through the inner Cr₂O₃ layer, due to nitrogen doping or local areas of nitride, or that conduction along the surface nitride across the coupon edges contributed to the low ICR values. Calculations suggest that the limited edge surface area would have

resulted in higher ICR values than those measured; however, further study and evaluation of this issue are planned.

An advantage of using oxidation to initially enrich the surface in chromium and vanadium prior to converting to nitride is that such selective oxidation may be accomplished at relatively low levels of chromium and vanadium due to the low solubility of oxygen in iron-based alloys and the high thermodynamic stability of Cr₂O₃ and V₂O₅. Although ICR and corrosion studies have only been pursued for nitrified Fe-27Cr-6V and Fe-27Cr-2V to date, it is estimated that the composition range amenable to this approach can likely be extended downward to ~15–20 wt.% chromium and 0.5–2 wt.% vanadium, which will lower alloy cost.

CHALLENGES AND FUTURE DIRECTIONS

The chromium-based nitride surfaces formed on Fe-27Cr-6V have not yet been evaluated in fuel cell testing. However, based on the single-cell test behavior of the thermally grown CrN/Cr₂N surfaces on the nitrified Ni-50Cr material, similar good performance is expected. Several key issues remain to be addressed to fully establish the potential of nitrified Fe-Cr-V alloys to meet DOE performance and durability goals.

First, to meet cost goals, metallic bipolar plates must be in the form of thin foil (0.1 mm range), and thermal nitridation could potentially warp or otherwise compromise the properties of stamped alloy foil bipolar plates. Preliminary assessment with stamped and nitrified Ni-Cr alloy foil suggested that significant warping does not occur;⁶³ however, the slight warping observed could cause issues with regards to sealing the edges of the fuel cell stack. Nitridation was, however, observed to embrittle thin Ni-Cr alloy foil under conditions where internal nitridation accompanied the external nitride layer formation.⁶³ The use of an initial oxide layer to limit internal nitrogen penetration and aid external nitride formation on vanadium-modified Fe-Cr based alloys should help ameliorate this issue.

Second, although single-cell fuel cell testing has indicated good durability for thermally grown CrN/Cr₂N surfaces, more aggressive conditions can

be encountered in fuel cell stacks. In particular, short-term local voltages in excess of 1V^{64,65} may occur under start-up conditions if oxygen gains access to the anode side of the cell. Corrosion current densities increased significantly for thermally grown CrN/Cr₂N surfaces above 0.8–0.9 V vs. SHE in polarization testing in sulfuric acid solutions (Figures 6 and 11). On nitrified Ni-50Cr, this increase was partially linked to oxygen incorporation in the form of a graded, mixed Cr-O/Cr-N-O species solid solution,⁵⁴ which does not appear to increase contact resistance, at least after short-term exposures. Taguchi and Kurihara⁶⁶ report increased corrosion current densities and transpassive dissolution of chromium metal and nitrified pure chromium as Cr₂O₇²⁻ in 1 kmol-m⁻³ sulfuric acid at 40°C at potentials higher than ~1.2V vs. SHE, which suggests that degradation of thermally grown chromium-nitride surfaces on Fe-Cr-V alloys may occur above 1V. Although such excursions greater than 1V may be for only a few seconds, their effects can accumulate per shut-down/start-up over time under automotive drive-cycle conditions. Approaches to reduce or eliminate transient high voltages on start-up are being pursued (e.g., Reference 65), and it should be noted that the MEA carbon catalyst supports are also attacked under these conditions. Fuel cell stack testing, including frequent shut-down/start-up cycles, is planned to evaluate these effects for nitrified Fe-Cr-V bipolar plates.

ACKNOWLEDGEMENTS

The authors thank B.A. Pint, J.H. Schneibel, G.J. Tatlock, and P.F. Tortorelli for helpful comments in reviewing this manuscript. Funding from the U.S. Department of Energy (DOE) Hydrogen, Fuel Cells, and Infrastructure program is gratefully acknowledged. Oak Ridge National Laboratory is managed by UT-Battelle, LLC for the U.S. DOE under contract DE-AC05-00OR22725.

References

1. J. Larminie and A. Dicks, *Fuel Cell Systems Explained* (West Sussex, England: John Wiley & Sons, Ltd., 2000).
2. R. Borup and N.E. Vanderborgh, *Mat Res. Soc. Symp. Proc. 393*, ed. D.H. Dougherty et al. (Warrendale, PA: Material Research Society, 1995), p. 151.
3. B.C.H. Steele and A. Heinzl, *Nature*, 414 (2001), pp. 345–352.

4. N.P. Brandon, S. Skinner, and B.C.H. Steele, *Ann. Rev. Mater. Res.*, 33 (2003), p. 183.

5. A. Hermann, T. Chaudhuri, and P. Spagnol, *Int. J. Hydrogen Energy*, 30 (2005), p. 1297.

6. Figure reproduced from Los Alamos National Laboratory, Fuel Cells—Green Power, LA-UR-99-3231, courtesy of the United States Department of Energy.

7. T.M. Besmann et al., *J. Electrochem. Soc.*, 147 (2000), pp. 4083–4086.

8. J. Scholta et al., *J. Power Sources*, 84 (1999), pp. 231–234.

9. D.P. Wilkinson et al., "Method of Fabricating an Embossed Fluid Flow Field Plate," U.S. patent 5,527,363 (18 June 1996).

10. N. Cunningham et al., *J. Electrochem. Soc.*, 149 (2002), pp. 905–911.

11. R.J. Lawrance, "Low Cost Bipolar Current Collector-Separator for Electrochemical Cells," U.S. patent 4,214,969 (29 July 1980).

12. E.N. Balko and R.J. Lawrance, "Carbon Fiber Reinforced Fluorocarbon-Graphite Bipolar Current Collector-Separator," U.S. patent 4,339,322 (13 July 1982).

13. D.N. Busick and M.S. Wilson, "Composite Bipolar Plates for Fuel Cells," *Proton Conducting Membrane Fuel Cells II*, Vol. 98-27 (Boston, MA: The Electrochemical Society, 1998), pp. 435–445.

14. M.S. Wilson and D.N. Busick, "Composite Bipolar Plate for Electrochemical Cells," U.S. patent 6,248,467 (19 June 2001).

15. J.H. Wang, D.G. Baird, and J.E. McGrath, *J. Power Sources*, 150 (2005), p. 110.

16. M.H. Abdelhamid et al., "Polymer Composite," U.S. patent application 20,040,062,974 (26 June 2003).

17. R.K.A.M. Mallant et al., *Program and Abstracts of the Fuel Cell Seminar* (Washington, D.C.: Fuel Cell Seminar Headquarters, 1994), p. 503.

18. R.G. Spear, H.H. Mueggenburg, and R. Hodge, "Metal Platelet Fuel Cells Production and Operation Methods," U.S. patent 5,683,828 (4 November 1997).

19. M.S. Wilson and C. Zawodzinski, "Fuel Cell with Metal Screen Flow-Field," U.S. patent 6,207,310 (27 March 2001).

20. D.R. Hodgson and E. Farndon, "Substrate Treatment," U.S. patent application 20,030,170,526 (4 February 2003).

21. B. May and D.R. Hodgson, "Fuel Cells and Fuel Cell Plates," U.S. patent application 20,010,021,470 (14 March 2001).

22. Q. Fan et al., "Low Cost Metal Bipolar Plates and Current Collectors for Polymer Electrolyte Membrane Fuel Cells," U.S. patent application 20,020,172,849 (6 April 2001).

23. Y. Tarutani et al., "Stainless Steel Product for Producing Polymer Electrode Fuel Cell," U.S. patent 6,379,476 (30 April 2002).

24. P.L. Hentall et al., *J. Power Sources*, 80 (1999), pp. 235–241.

25. A. Pozio et al., *Electrochimica Acta*, 48 (11) (2003), pp. 1543–1549.

26. R.C. Makkus et al., *J. Power Sources*, 86 (2000), p. 274.

27. D.P. Davies et al., *J. Appl. Electrochem.*, 30 (2000), pp. 101–105.

28. H. Wang, M. Sweikart, and J.A. Turner, *J. Power Sources*, 115 (2003), pp. 243–251.

29. H. Wang and J.A. Turner, *J. Power Sources*, 128 (2004), p. 193.

30. H. Wang, G. Teeter, and J.A. Turner, *J. Electrochem. Soc.*, 153 (3) (2005), p. B99.

31. C.L. Ma, S. Warthesen, and D.A. Shores, *J. New Mater. Electrochem. Sys.*, 3 (2000), p. 221.

32. J. Wind et al., *J. Power Sources*, 105 (2002), p. 256.

33. Y. Li et al., "Corrosion Resistant PEM Fuel Cell," U.S. patent 5,624,769 (29 April 1997).

34. S. Joseph et al., *Int. J. Hydrogen Energy*, 30 (12) (2005), p. 1339.

35. M. Li et al., *Corr. Sci.*, 46 (2004), pp. 1369–1380.

36. S.J. Lee, C.H. Huang, and Y.P. Chen, *J. Mater. Process. Tech.*, 140 (2003), pp. 688–693.

37. N. Aukland et al., *J. Mater. Res.*, 19 (6) (2004), p. 1723.

38. M.H. Abdelhamid, R.H. Blunk, and G. Vyas, "Enhanced Stability Bipolar Plate," U.S. patent application 20,060,019,142 (26 January 2006).

39. *The Hydrogen, Fuel Cells & Infrastructure Technologies Program Multi-Year Research, Development and Demonstration Plan* (Washington, D.C.: U.S. Department of Energy, February 2005), pp. 3–89; <http://www1.eere.energy.gov/hydrogenandfuelcells/mypp/>.

40. W. Brandl and C. Gendig, *Thin Solid Films*, 343 (1996), pp. 290–291.

41. K. Weisbrod, D. Prier II, and N. Vanderborgh, *FY1999 Progress Report for Fuel Cells For Transportation Proceedings, Energy Efficiency and Renewable Energy Review* (Washington, D.C.: U.S. Department of Energy, 1999), p. 117.

42. K.S. Weil et al., "Development of Low-Cost, Clad Metal Bipolar Plates for PEM Fuel Cells," *2005 Annual Progress Report, DOE Hydrogen, Fuel Cells, and Infrastructure Program*, www.hydrogen.energy.gov/annual_progress05_fuelcells.html#d.

43. M.P. Brady et al., *Electrochem. and Solid-State Lett.*, 5 (2002), pp. 245–247.

44. S. Seal, *JOM*, 53 (9) (2001), p. 51.

45. P. Kofstad, *High Temperature Corrosion* (London: Elsevier Applied Science Publishing, 1988).

46. M.P. Brady, B. Gleeson, and I.G. Wright, *JOM*, 52 (1) (2000), pp. 16–21.

47. G.Y. Lai, *High-Temperature Corrosion of Engineering Alloys* (Materials Park, OH: ASM International, 1990), p. 75.

48. D.R. Sigler, *Oxid. Met.*, 32 (5/6) (1989), pp. 337–355.

49. R.A. Rapp, *Corrosion*, 21 (1965), pp. 382–401.

50. M.P. Brady et al., *Materials and Corrosion*, 56 (11) (2005), pp. 748–755.

51. G.C. Savva, G.C. Weatherly, and J.S. Kirkaldy, *Met. Mater. Trans. A*, 27 (6) (1996), pp. 1611–1622.

52. H.J. Christ, S.Y. Chang, and U. Krupp, *Materials and Corrosion*, 54 (11) (2003), pp. 887–894.

53. R.P. Rubly and D.L. Douglass, *Oxid. Met.*, 35 (3-4) (1991), pp. 259–278.

54. I. Paulauskas et al., "Corrosion Behavior of CrN, Cr₂N and Pt Phase Surfaces Formed on Nitrided Ni-50Cr with Application to Proton Exchange Membrane Fuel Cell Bipolar Plates," *Corrosion Science* (in press).

55. M.P. Brady et al., *Scripta Mat.*, 50 (7) (2004), pp. 10–17.

56. H. Wang et al., *J. Power Sources*, 138 (2004), pp. 86–93.

57. A.A. Kodentsov et al., *Metal. and Mater. Trans. A*, 27 (1996), pp. 59–69.

58. U. Krupp, S.Y. Chang, and H.-J. Christ, *Z. Metallkunde*, 91 (2000), pp. 1006–1012.

59. N. Ono, M. Kajihara, and M. Kikuchi, *Met. Trans. A*, 23 (1992), pp. 1389–1393.

60. H. Wang et al., *J. Power Sources*, 138 (2004), p. 79.

61. B. Yang et al., to be submitted to *Acta Materialia*.

62. H. Kuwamoto, J.M. Honig, and J. Appel, *Phys. Rev. B*, 22 (1980), p. 2626.

63. M.P. Brady et al., "Cost-Effective Surface Modification for Metallic Bipolar Plates," *2005 Annual Progress Report, DOE Hydrogen, Fuel Cells, and Infrastructure Program*, www.hydrogen.energy.gov/annual_progress05_fuelcells.html#d.

64. C.A. Reiser et al., *Electrochemical and Solid State Letters*, 8 (6) (2005), pp. A273–A276.

65. T.A. Bekkedahl et al., "Reducing Fuel Cell Cathode Potential during Startup and Shutdown," U.S. patent application 20,040,081,866 (2004).

66. M. Taguchi and J. Kurihara, *Materials Transactions*, 32 (1991), pp. 1170–1176.

M.P. Brady, B. Yang, and K.L. More are with Oak Ridge National Laboratory in Tennessee; H. Wang and J.A. Turner are with National Renewable Energy Laboratory in Golden, Colorado; and M. Wilson and F. Garzon are with Los Alamos National Laboratory in New Mexico.

For more information, contact M.P. Brady, Oak Ridge National Laboratory, 1 Bethel Valley Road, Oak Ridge, TN 37831-6115; (865) 574-5153; fax (865) 241-0215; e-mail bradyp@ornl.gov.

Reader Services

TO SUBSCRIBE, PRINT OR ELECTRONIC:

- Telephone: 1-800-759-4867 within the U.S. (724) 776-9000 ext. 251
- E-mail: publications@tms.org
- On the web: doc.tms.org

TO REPORT A PROBLEM WITH YOUR SUBSCRIPTION:

- Telephone: (724) 776-9000 ext. 251
- E-mail: mcirelli@tms.org

TO OBTAIN BACK ISSUES:

- Telephone: (724) 776-9000 ext. 251
- Fax: (724) 776-3770
- E-mail: mcirelli@tms.org

TO CHANGE YOUR ADDRESS:

- Telephone: (724) 776-9000 ext. 241
- On the web: members.tms.org

TMS MEMBERS:
Access JOM on-line at no charge by visiting members.tms.org

TO SUBMIT AN ARTICLE:

- Check the listing of upcoming editorial topics at www.tms.org/pubs/journals/JOM/techcalendar.html
- Develop a 300-word abstract, including probable title and brief biographical sketch
- Submit the abstract via the web at www.tms.org/pubs/journals/JOM/abstract-author.html or by fax at (724) 776-3770

TO OBTAIN REPRINTS:

- Reprints are available for a fee one month after the issue is released
- For information contact Mark Cirelli by e-mail at mcirelli@tms.org or by telephone at (724) 776-9000 ext. 251

TO OBTAIN PERMISSION TO REPRINT AN ARTICLE:

- Contact Trudi Dunlap by e-mail at tdunlap@tms.org or by telephone at (724) 776-9000 ext. 275

TO ACQUIRE AN INDIVIDUAL PAPER IN PORTABLE DOCUMENT FORMAT:

- Visit the document center at doc.tms.org

JOM Web Site: www.tms.org/jom.html

JOM, 184 THORN HILL ROAD, WARRENDALE, PA 15086